Mach-Zehnder silicon photonic modulator assisted by phase-shifted Bragg gratings
— **Source link** ↗

Omid Jafari, Wei Shi, Sophie LaRochelle

Institutions: Laval University

Published on: 05 Mar 2020 - IEEE Photonics Technology Letters (IEEE)

Topics: Fiber Bragg grating, Phase modulation, Silicon photonics, Mach–Zehnder interferometer and Resonator

Related papers:

- High-Efficiency Silicon Photonic Modulator Using Coupled Bragg Grating Resonators

- Silicon-on-Insulator Modulators Using a Quarter-Wave Phase-Shifted Bragg Grating

- DAC-Less PAM-4 Slow-Light Silicon Photonic Modulator Providing High Efficiency and Stability

- Silicon Photonic Modulator based on Coupled Bragg Grating Resonators used as Phase Shifters

- DAC-Less PAM-4 Slow-Light Silicon Photonic Modulator Assisted by Coupled Bragg Grating Resonators

Mach-Zehnder Silicon Photonic Modulator Assisted by Phase-Shifted Bragg Gratings

Omid Jafari, *Student Member, IEEE*, Wei Shi, *Member, IEEE*, and Sophie LaRochelle, *Senior Member, IEEE*

Abstract— **We experimentally demonstrate a silicon photonic Mach-Zehnder modulator (MZM) assisted by phase-shifted Bragg gratings. Coupled resonators are inserted in the Bragg grating structure to significantly enhance the phase modulation efficiency, while maintaining a wide optical bandwidth compared to other resonator-based modulators. Fabricated using a CMOS-compatible foundry process, the device achieved a small-signal $V_\pi L$ of 0.18 V.cm, which is seven times lower than a conventional silicon MZM fabricated with the same process. The device has a compact footprint, with a length of only 162 μm, and shows a modulation bandwidth of 28 GHz at a reverse bias of 1 V. Non-return-to-zero modulation is demonstrated at 30 Gb/s with a bit-error-rate (BER) below the 7%-overhead forward error correction (FEC) threshold over a bandwidth of 3.5 nm. This bandwidth should translate into an operating temperature range greater than 40 ^{0}C.**

Index Terms—**Electro-optic modulators, Optical resonators, Bragg gratings, Modulation enhancement, Silicon photonics.**

I. INTRODUCTION

Optical modulators are key components for optical interconnects that require low-cost photonic integrated circuits (PICs). Silicon photonic (SiP) modulators are thus considered a preferred candidate for this application because of their compatibility with CMOS manufacturing processes. There are currently two general categories of SiP modulators: MZMs and resonance-based modulators (RBMs). Because of intrinsic trade-offs, none of these meet all of the performance criteria required for future data centers, such as high modulation bandwidth and low energy-per-bit. MZMs have been extensively studied for high-speed modulation as they offer a wide optical bandwidth and temperature-insensitive operation [1]. In addition, when operated in a push-pull configuration, MZMs enable the generation of chirp-free pulses. Despite these advantages, SiP MZMs are hindered by their low efficiency, resulting in a large footprint and high energy consumption [1]. By enhancing phase modulation, resonators allow a drastic reduction of the phase shifter length. For example, micro-ring modulators (MRMs) have a very compact footprint and low power consumption [2], [3]. Still, these benefits come with several challenges. Firstly, the operational spectral bandwidth is quite narrow and a small temperature variation can cause an important degradation in the performance. Secondly, MRMs suffer from a strong chirp. Thirdly, the narrow resonance also limits the EO bandwidth due to the long photon lifetime associated with resonators with high-quality factor.

Combining resonators to a Mach-Zehnder interferometer (MZI) is a promising method to overcome the low modulation efficiency of conventional MZMs [4]–[6]. However, the modulation enhancement is obtained at the price of increased temperature sensitivity, similarly to MRMs. The introduction of cascaded rings in each arm of the MZI was proposed to enlarge the operating temperature range but the free spectral range (FSR) limitation of this design prevents its use in wavelength division multiplexing (WDM) applications [7]. In [8], MZMs are loaded with 2D photonic crystal waveguides (PCWs) to achieve a high modulation efficiency with a large optical bandwidth. Fabrication of 2D-PCW is however well known to be very challenging using standard CMOS manufacturing processes since the design incorporates small features that tend to be smoothed by the optical lithography. Bragg grating devices, which are 1-D PCW, are less sensitive to fabrication errors and are routinely fabricated using UV lithography. In [9], [10], Bragg gratings were inserted in each arm of a MZI to enhance modulation through the slow-light effect. However, only small delay-bandwidth products were reported.

In [11], we proposed a novel design of a MZM assisted by integrated Bragg grating resonators (IBGRs). When operated in the low-dispersion-slow-light regime, the IBGRs can significantly enhance the modulation efficiency of MZM. Also, we showed that these structures can be engineered to have a larger optical bandwidth in order to increase modulation stability and robustness with respect to temperature variations. In this paper, we experimentally demonstrate, for the first time, an MZM assisted by IBGRs. The modulator was fabricated with a CMOS-compatible foundry process. Experimental results show a small-signal $V_\pi L$ much smaller than conventional MZM and a high EO bandwidth.

II. DESIGN AND MODULATOR STRUCTURE

Figure 1 (a) shows the modulator schematic. In [11], we discussed how to engineer the IBGR slow-light effect, taking into account the tradeoff between efficiency and stability. The key idea is to ensure that the resonance optical bandwidth remains large by employing cavities with a low-quality factor. The required phase modulation is then obtained by cascading such resonators. The modulator offers a compact footprint and low power consumption (similar to MRM). It also presents a stable operation and a high EO bandwidth (similar to conventional MZM), achieving a balance in the performance. An IBGR, with a uniform period of Λ=300 nm and six-coupled resonators, is placed in each arm of the MZM. Each resonator consists of a phase-shifted section with 45 grating periods on

[1]Centre d'optique, photonique et laser (COPL), Department of Electrical and Computer Engineering, Université Laval, Québec, QC, G1V 0A6, Canada. Email: sophie.larochelle@gel.ulaval.ca
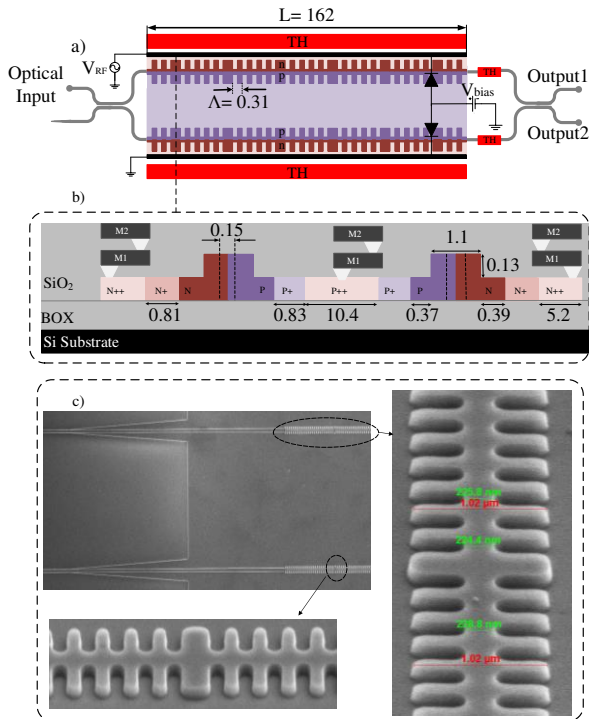
Fig. 1. a) Modulator schematic, b) modulator cross-section, c) SEM picture of the two arms with their resonators. (Dimensions in a) and b) are in μm).
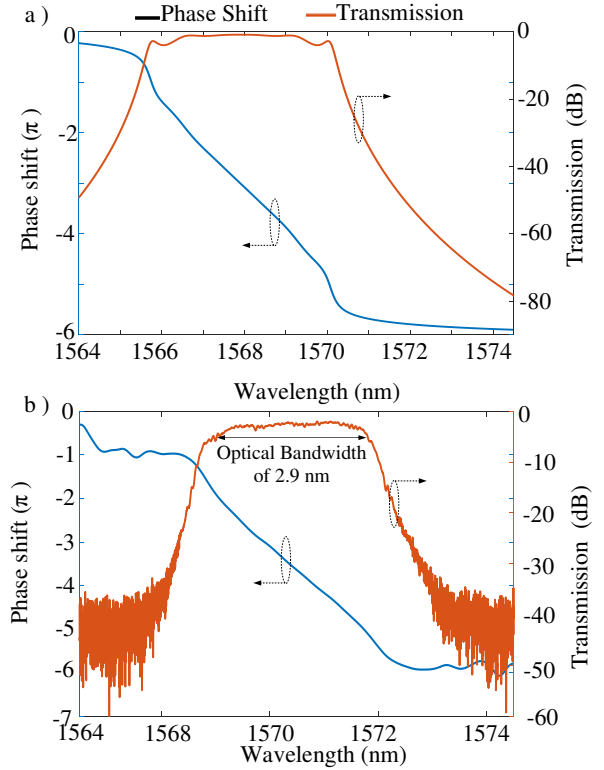

Fig. 2. a) Simulated transmission amplitude and phase responses of the IBGR b) Transmission amplitude and phase responses of the IBGR measured with a LUNA OVA.

each side. The Bragg gratings consist of sidewall corrugations with a duty cycle of 50% in a ridge waveguide having an average width of 625 nm, a ridge height of 220 nm and a slab height of 90 nm. The maximum and minimum widths are 1100 nm and 150 nm, respectively. Such ultra-large corrugations allow us to keep the number of grating periods low, resulting in a short phase shifter length. Fig. 1 (b) shows the symmetric lateral p-n junctions and the three doping levels used to minimize optical loss and keep the resistance low.

Because of fabrication imperfections, four thermal elements are included in the design to adjust the modulator. We placed two thermal elements on top of the IBGRs to match their stopbands. In each arm, we also put a thermal element to bias the modulator at the quadrature point. Also, we placed an on-chip 50 Ω load between RF pads for impedance matching. The modulator was fabricated in a multi-project wafer run using a standard 193 nm lithography process at the IME (AMF) A*STAR with a silicon layer thickness of 220 nm and a 2 μm buried oxide. Fig. 1 (c) shows SEM pictures of parts of the fabricated modulator.

III. EXPERIMENT

A. Transmission Spectrum

Figure 2 (a) illustrates the simulated transmission amplitude and phase of the IBGR close to the resonance peak (see [11] for details). The simulated resonant peak has a bandwidth of 4 nm; however, the measured spectrum (in Fig. 2 (b)) shows only a 2.9 nm bandwidth. This difference can be explained by fabrication errors that result in the resonators of the IBG structure not being perfectly matched, i.e., not having the same central wavelength. The MZI response shows that the

quadrature point at 1570 nm is obtained by applying a voltage of 1.9 V to the heater of the bottom arm. The extinction ratio (ER) of the MZI structure is 28 dB.

B. Modulation Efficiency

The phase-shifted IBGs are operated in transmission as phase modulators, and therefore they must be placed into a MZI to produce amplitude modulation. Assuming ideal directional couplers, the MZI output is given by,

$$P_{out} = P_{in} \exp(-\alpha L)\cos^2(\Delta\varphi_v), \quad \Delta\varphi_v = \frac{k_0 \Delta n_{eff}(V)\gamma L + \Delta\varphi_0}{2} \quad (1)$$

where P_{in} is the input power and α is the propagation loss coefficient. The total phase difference between the two MZI arms is $\Delta\varphi_v$, where $\Delta\varphi_0$ represents the initial phase difference between the two arms, and Δn_{eff} is the modulation of the waveguide effective refractive index with applied voltage. The factor γ is named the enhancement factor as it represents the phase modulation enhancement produced by the IBGR compared to a simple phase shifter in a rib waveguide of the same length. Finally, k_0 is the wavenumber equal to $2\pi/\lambda_0$. The modulation efficiency can be evaluated by the typical figure of merit ($V_\pi \times L$) and the required energy per bit.

The on-chip 50 Ω termination does not allow us to measure the large-signal $V_\pi \times L$. That is because, when applying DC voltages to RF pads, the DC current passing through the termination causes a change in the temperature of the chip, resulting in an unwanted shift in the optical spectrum. Therefore, to avoid heating caused by large-signal $V_\pi \times L$, we provide an estimation of V_π by applying a small signal at a low
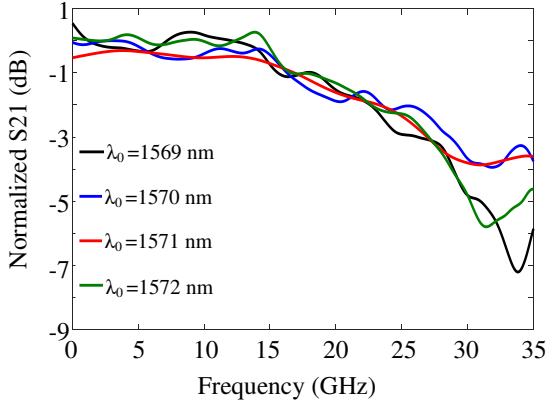
Fig. 3. Measured EO scattering parameter S_{21} for different operational wavelengths at a reverse bias of 1V.
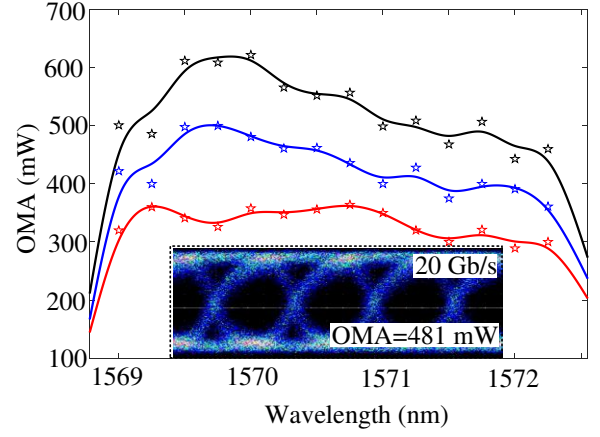

Fig. 4. OMA spectra measured for bitrates of 10 Gb/s (black curve), 20 Gb/s (blue curve), and 30 Gb/s (red curve) at a V_{bias} of -1.5 V. Symbols are experimental measurements, the curves are guides for the eye. The inset is the eye diagram for a bitrate of 20 Gb/s.

frequency; and we assume that the variation of phase as a function of voltage is linear around the bias point. Using this approach, the modulator records a small-signal $V_\pi \times L$ of 0.18 V.cm. For the purpose of comparison, we perform a similar measurement on a conventional MZM that has been fabricated with the same manufacturing process. Note that the p-n junctions of both modulators are identical. The conventional MZM is characterized by a small-signal $V_\pi \times L$ of 1.27 V.cm. This shows that the IBGR structure provides an enhancement factor of $\gamma=7$, or, in other words, this means that the length of its phase shifters can be seven times shorter.

In order to compare our structure with the other Bragg-grating-based MZMs [9], [10], we refer to delay-bandwidth product (or γ-bandwidth product). Note that a larger enhancement factor means a larger delay. Reference [9] reported a γ-bandwidth product of 2.6 nm (enhancement factor of 2 and optical bandwidth of 1.3 nm); also reference [10] demonstrated two γ-bandwidth products of 12 nm (enhancement factor of 3 and optical bandwidth of 4 nm) and 4.8 nm (enhancement factor of 6 and optical bandwidth of 0.6 nm). Our modulator provides the enhancement factor of 7 while the optical bandwidth is 2.9 nm, recording a γ-bandwidth product of 20.3 nm. Furthermore, our modulator has much more compact footprint (L=162 µm) compared to references [9] (L=500 µm), and [10] (L=2000 µm).

The energy consumption per bit of the modulator for the OOK modulation format is calculated by $E_b=1/4\ CV_{pp}^2$. The p-n junction model shows that the capacitance of the p-n junctions at the reverse bias (V_{bias}) of 1.5 V is 1.7 pF/cm [11]. Considering a 162 µm phase shifter length, the total capacitance is 27.5 fF. As a result, the estimated power consumption is 84 fJ/bit.

C. Loss

The total on-chip loss is 22.5 dB, of which 17 dB comes from the un-optimized grating couplers and fiber arrays, 1 dB from the two 3-dB adiabatic couplers, 2.5 dB propagation loss from 1 cm-long routing waveguide, and 2 dB from the modulator (i.e., propagation loss of 123 dB/cm for IBGRs).

D. EO Bandwidth

Figure 3 shows EO bandwidth of the modulator at V_{bias} of -1 V measured with the PNA Microwave Network Analyzer
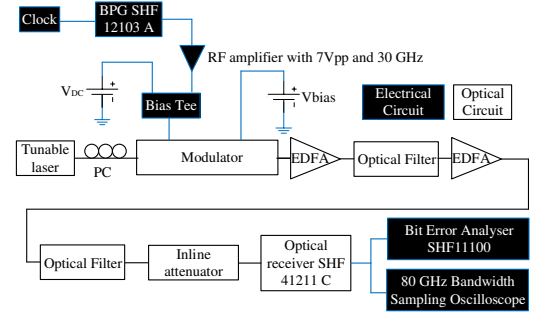

Fig. 5.Setup used to measure OMA, BER, and eye diagram.

(Agilent N5227A 10 MHz - 67 GHz). The 3-dB bandwidth is about 28 GHz for different operational wavelengths. The EO bandwidth is usually described by considering the photon lifetime of the IBGR, $1/(2\pi f_\tau)$, and the RC time constant of the p-n junction, $1/(2\pi f_{RC})$. We write $(1/f_0)^2=(1/f_{RC})^2+(1/f_\tau)^2$, where f_0 is 3-dB EO bandwidth of the modulator. The RC time constant of the modulator modeled in [11] is equal to 2.8 ps for V_{bias} of -1 V, resulting in cut-off frequency $f_{RC}=1/(2\pi RC)$ of ~55 GHz. From the measured EO bandwidth and the calculated f_{RC}, we estimate that $f_\tau=1/(2\pi\tau)$ of ~32.5 GHz, which corresponds to a photon lifetime of approximately 5 ps. Fig. 3 (b) also shows that the small-signal bandwidth of the modulator is similar over a wavelength range of 3 nm, which should reduce the modulator sensitivity to the temperature variations compared to usual RBMs.

E. Optical Modulation Amplitude (OMA) and Modulator Stability

To evaluate the quality of the modulated signal, we measured the OMA of the modulator. The OMA is computed using $OMA=P_1-P_0$, where P_1 and P_0 are output powers corresponding to bit "1" and bit "0", respectively. Fig. 4 displays the OMA spectra for different bitrates measured on a commercial optical receiver (SHF 41211 C) that has an internal RF amplifier. Fig. 4 shows that the modulator exhibits good performance in terms of OMA over a wavelength range of 3.5 nm. Considering a typical resonant shift of 80 pm/^{0}C [2], the operating temperature
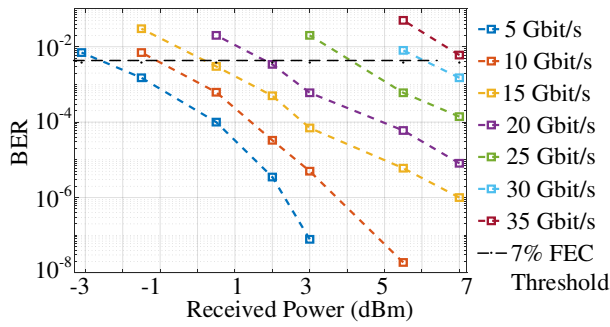
Fig. 6. BER as a function of the received power for different bitrates. Results are measured at V_{bias} of -1.5 V and operational wavelength of 1570 nm.

Fig. 7. BER vs. wavelength for different bitrates at V_{bias} of -1.5 V.

range of the modulator is estimated to be larger than 40 ^{0}C. Compared to single-resonator modulators such as MRM, the requirement on the thermal control is significantly relaxed, leading to reduced cost and control-circuit complexity.

F. Large-Signal Performance

The modulator performance was evaluated with an OOK modulation format using the setup shown in Fig. 5. We first generate a pseudo-random bit sequence with a length of 2^{31}-1 using a bit pattern generator (BPG) (SHF 12103 A). Next, the signal is amplified by a 30 GHz bandwidth RF amplifier (SHF 807), resulting in a peak-to-peak modulation voltage of 3.5 V on each arm of the modulator.

The input laser signal, with a power of 15 dBm goes through a polarization controller (PC) to improve fiber-to-chip coupling in the fundamental TE mode. After modulation, the signal is amplified by two stages of erbium-doped fiber amplifier (EDFA) and tunable optical bandpass filter (TOBP). An inline attenuator controls the signal power at the optical receiver (SHF 41211 - 32 GHz). We use an 80 GHz bandwidth sampling oscilloscope and a bit-error-rate analyzer (SHF 11100 B) to respectively capture the eye-diagrams and measure the BER. Note that all of the results are obtained without digital signal processing (DSP).

The inset of Fig. 4 shows the eye diagram of the modulated signal at 20 Gb/s. BER curves, measured as a function of the received power at λ_0 of 1570 nm and V_{bias} of -1.5 V, are shown in Fig. 6. Assuming a 7 % FEC threshold, the modulator provides error-free operation up to 30 Gb/s. Fig. 7 shows the measured BER as a function of wavelength for different modulation speeds, clearly showing that the modulator can be operated over a wavelength range of 3.5 nm with a BER below the 7% FEC threshold. This bandwidth should provide an operating temperature range > 40 ^{0}C as previously discussed.

IV. Conclusion

We experimentally demonstrated a MZM assisted by coupled resonators in an IBG structure that significantly improves modulation efficiency and footprint. The results are obtained using low-quality-factor resonators in order to have an operating range of several nanometers. The use of coupled resonators provides more degrees of freedom for optimization and leads to significant improvement over previous demonstration. This modulator is thus characterized by a low
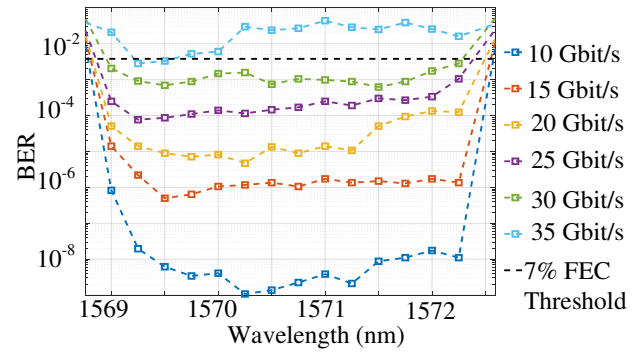
power consumption (84 fJ/bit), an improved modulation efficiency (small-signal $V_\pi \times L$= 0.18 V.cm), and a compact footprint (L=162 μm). The BER measurement shows that the modulator can be operated up to 30 Gb/s below the 7% FEC threshold and that it should be stable over a temperature range larger than 40 ^{0}C.

References

[1] D. Patel, S. Ghosh, M. Chagnon, A. Samani, V. Veerasubramanian, M. Osman, and D. V. Plant, "Design, analysis, and transmission system performance of a 41 GHz silicon photonic modulator," *Opt. Express*, vol. 23, no. 11, pp. 14263-14287, 2015.

[2] R. Dubé-Demers, S. LaRochelle, and W. Shi, "Ultrafast pulse-amplitude modulation with a femtojoule silicon photonic modulator," *Optica*, vol. 3, no. 6, pp. 622-627, 2016.

[3] M. S. Hai, M. M. P. Fard, and O. Liboiron-Ladouceur, "A Ring-Based 25 Gb/s DAC-Less PAM-4 Modulator," *IEEE J. Sel. Top. Quantum Electron.*, vol. 22, no. 6, pp. 123–130, 2016.

[4] R. Li, D. Patel, A. Samani, E. El-Fiky, Z. Xing, M. Sowailem, Q. Zhong, and D. V. Plant, "An 80 Gb/s Silicon Photonic Modulator Based on the Principle of Overlapped Resonances," *IEEE Photonics J.*, vol. 9, no. 3, pp. 1-11, 2017.

[5] J. Cardenas, P. A. Morton, J. B. Khurgin, A. Griffith, C. B. Poitras, K. Preston, and M. Lipson, "Linearized silicon modulator based on a ring assisted Mach Zehnder inteferometer," *Opt. Express*, vol. 21, no. 19, pp. 22549-22557, 2013.

[6] A. M. Gutierrez, A. Brimont, G. Rasigade, M. Ziebell, D. Marris-Morini, J-M. Fedeli, L. Vivien, J. Marti, and P. Sanchis, "Ring-Assisted Mach–Zehnder Interferometer Silicon Modulator for Enhanced Performance," *J. Light. Technol.*, vol. 30, no. 1, pp. 9-14, 2012.

[7] S. Romero-García, A. Moscoso-Mártir, S. S. Azadeh, J. Müller, B. Shen, F. Merget, and J. Witzens, "High-speed resonantly enhanced silicon photonics modulator with a large operating temperature range," *Opt. Lett.*, vol. 42, no. 1, pp. 81-84, 2017.

[8] Y. Terada, K. Kondo, R. Abe, and T. Baba, "Full C-band Si photonic crystal waveguide modulator," *Opt. Lett.*, vol. 42, no. 24, pp. 5110-5112, 2017.

[9] A. Brimont *et al.*, "High-contrast 40 Gb/s operation of a 500 μm long silicon carrier-depletion slow wave modulator," *Opt. Lett.*, vol. 37, no. 17, pp. 3504-3506, 2012.

[10] R. Hosseini, L. Mirzoyan, and K. Jamshidi, "Energy Consumption Enhancement of Reverse-Biased Silicon-Based Mach–Zehnder Modulators Using Corrugated Slow Light Waveguides," *IEEE Photonics J.*, vol. 10, no. 1, pp. 1-7, 2018.

[11] O. Jafari, H. Sepehrian, W. Shi, and S. LaRochelle, "High-Efficiency Silicon Photonic Modulator Using Coupled Bragg Grating Resonators," *J. Light. Technol.*, vol. 37, no. 9, pp. 2065-2075, 2019.